A Brownian Oscillator Approach to the Kennard−Stepanov Relation

Y. Zhao[†] and R. S. Knox*

Rochester Theory Center for Optical Science and Engineering and Department of Physics and Astronomy, University of Rochester, Rochester, New York, 14627-0171

Received: May 3, 2000

The Kennard−Stepanov (KS) relation, also known as the reciprocity relation, connects the absorption and fluorescence spectra of homogeneous complex systems under the assumption of thermal equilibration of the emitting electronic state. A recent elaboration of the theory by Sawicki and Knox (SK) [*Phys. Rev. A,* **1996** *54,* 4837] introduces a spectral temperature that is a sensitive indicator of the failure of the relation. Studies using the SK formalism, which have been limited almost exclusively to experimental cases, reveal various failures that may be due to incomplete equilibration, inhomogeneity, or both. Using the Brownian oscillator model for nuclear dynamics, we investigate the KS relation theoretically with the aid of the SK spectral temperature. The spectral temperature is again found to be a sensitive indicator, this time of the accuracy of the numerical methods necessary for the multiple integrations. The original KS relation appears to hold regardless of the memory effects of the bath, a result which is not totally unexpected considering the assumptions of excited-state equilibrium implicit in the theory. We extend the theory to the nonequilibrated case of time-resolved fluorescence, where a time-dependent temperature can be defined.

I. Introduction

As a consequence of the Einstein relation which connects the rates of spontaneous emission, stimulated emission, and absorption of radiation between microstates, the Kennard−Stepanov (KS) relation[1−3] connects the steady-state absorption and fluorescence spectra of a two-level chromophore at temperature T

$$F(\omega) = \ln\frac{I(\omega)}{\sigma(\omega)} = \frac{\hbar\omega_{eg} - \hbar\omega}{k_B T} + D(T) \qquad (1.1)$$

Here $\hbar\omega_{eg}$ is the electronic energy of excitation, k_B is Boltzmann's constant, and $I(\omega)$ and $\sigma(\omega)$ are the emission and absorption line shape functions at frequency ω, respectively. $D(T)$, which is determined by the partition functions of the ground and excited manifolds,[4] does not depend on this frequency. In addition to making use of the Einstein relation, the KS relation assumes that the excited state is thermally equilibrated before emission. Therefore, violation of the KS relation has been frequently used to infer deviation from thermal equilibrium of the excited manifold. An effective temperature termed the spectral temperature was introduced by Sawicki and Knox[5] using the local slope of $F(\omega)$

$$T^*(\omega) = -\left[\frac{k_B}{\hbar}\frac{dF}{d\omega}\right]^{-1} \qquad (1.2)$$

KS theory also assumes that the spectra under consideration involve no transitions between vibrational levels of the ground states.

Experimentally, T^* is seldom found to agree with the ambient temperature T, although the KS relation is commonly used in the field of biofluorescence (see, for example, refs 6−8). The function $F(\omega)$ derived from measurements is often a nearly straight line; however, it has long been a puzzle that T^* is higher than the ambient temperature T in some instances and lower in others.[9] The connection of $T^*(\omega)$ to relaxation among internally equilibrated but kinetically interacting manifolds is easily demonstrated.[9,10] The open question is: can $T^*(\omega)$ be related to relaxation *within* the excited manifold by use of relatively modern techniques such as applying the Brownian oscillator model? In this paper we set up and test a formalism for answering this question. In section II, we introduce the Brownian oscillator model. Defining various variables for discussion, we present expressions for the line shape function $g(t)$, from which we later obtain the linear absorption and the relaxed fluorescence line shapes. The line shape function must in turn be obtained from a correlation function derived from a model of the system. In section III this function is discussed in detail, and we use an oscillator continuum model as an example for which a closed expression for $g(t)$ can be derived. We discuss the implications of non-Ohmic relaxation in the baths. In section IV, we illustrate absorption line shapes for different parameter regimes and show numerically that for a frequency-independent damping constant the KS relation holds regardless of the damping strength as compared to the oscillator frequency. We demonstrate the behavior of T^* during the approach to thermal equilibrium in section V by calculating time-resolved fluorescence. Section VI is our summary.

II. The Brownian Oscillator Model

Huang and Rhys[11] were the first to treat a many-coordinate (many-body) system quantum mechanically in their description of optical properties of F centers. Their work was later extended to acoustic phonons by Lax.[12] However, polaron theories of chromophores coupled to a discrete set of coherent oscillators[13] miss an important aspect of the real system, namely, dissipation.

[†] Present address: Department of Chemistry, University of Hong Kong, Pokfulam Road, Hong Kong, China

10.1021/jp001686k CCC: $19.00 © 2000 American Chemical Society
Published on Web 07/20/2000

Therefore, such theories are incapable of describing the interesting phenomenon of excited-state relaxation. The Brownian oscillator model[14−17] introduces dissipation mechanisms into the harmonic quantum oscillators by coupling the primary oscillators to a continuous distribution of secondary oscillators.

In the Brownian oscillator model, the system is taken to be a two electronic-level system with some primary nuclear coordinates coupled linearly to the electronic systems:

$$H = |g\rangle H_g\langle g| + |e\rangle H_e\langle e| + H' \tag{2.1}$$

where

$$H_g = \sum_j \left[\frac{p_j^2}{2m_j} + \frac{1}{2}m_j\omega_j^2 q_j^2\right] \tag{2.2}$$

$$H_e = \hbar\omega_{eg}^0 + \sum_j \left[\frac{p_j^2}{2m_j} + \frac{1}{2}m_j\omega_j^2 (q_j + d_j)^2\right] \tag{2.3}$$

and

$$H' = \sum_n \left[\frac{P_n^{\,2}}{2m_n} + \frac{1}{2}m_n\omega_n^2\left(Q_n - \sum_j \frac{c_{nj}q_j}{m_n\omega_n^2}\right)^2\right] \tag{2.4}$$

Here p_j (P_n), q_j (Q_n), m_j (m_n), and ω_j (ω_n) represent the momentum, the coordinate, the mass, and the angular frequency of the jth (nth) nuclear mode of the primary (bath) oscillators, respectively. d_j is the displacement for the jth nuclear mode in the excited electronic state. H' describes the bath oscillators and their coupling to the primary oscillators with a coupling strength c_{nj}.

The linear absorption and the relaxed fluorescence line shapes can be obtained from a spectral broadening function $g(t)$ (see ref 14, Appendix 8B therein):

$$\sigma_{BO}(\omega) = \frac{1}{\pi}\mathrm{Re}\int_0^\infty \mathrm{d}t\, \exp[i(\omega - \omega_{eg}^0 - \lambda)t - g(t)]$$

$$I_{BO}(\omega) = \frac{1}{\pi}\mathrm{Re}\int_0^\infty \mathrm{d}t\, \exp[i(\omega - \omega_{eg}^0 + \lambda)t - g^*(t)] \tag{2.5}$$

where ω_{eg}^0 is the 0−0 transition frequency, λ is the Stokes shift, and $g(t)$ is related to the polarization of the material system as follows.

A Taylor expansion of the polarization in powers of the radiation field $E(\mathbf{r},t)$ is made:

$$P(\mathbf{r},t) = P^{(1)}(\mathbf{r},t) + P^{(2)}(\mathbf{r},t) + P^{(3)}(\mathbf{r},t) + ... \tag{2.6}$$

The term $P^{(1)}(\mathbf{r},t)$ is responsible for linear optics. We define the linear response function $S^{(1)}(\mathbf{r},t)$ as the first-order susceptibility through the polarization $P^{(1)}(\mathbf{r},t)$:

$$P^{(1)}(\mathbf{r},t) = \int_0^\infty \mathrm{d}t_1 S^{(1)}(\mathbf{r},t_1)E(\mathbf{r},t - t_1) \tag{2.7}$$

(The polarization and field are both vectors, but since we will not consider anisotropic systems, we do not use any special notation.) For the model system we are discussing, the susceptibility takes the form (ref 14, pp 116−120)

$$S^{(1)}(t_1) = \frac{i}{\hbar}\theta(t)[R(t) - R^*(t)] \tag{2.8}$$

where

$$R(t) = \exp(-i\omega_{eg}t)\exp[-g(t)] \tag{2.9}$$

and

$$\omega_{eg} = \omega_{eg}^0 + \langle U\rho_g\rangle \tag{2.10}$$

Here $U \equiv H_e - H_g$ is the collective bath coordinate representing the coupling of the chromophore to its environment responsible for spectral shifts and broadening, and ρ_g is the equilibrium ground-state density matrix:

$$\rho_g = \frac{|g\rangle\langle g|\exp(-\beta\hat{H}_g)}{Tr[\exp(-\beta\hat{H}_g)]} \tag{2.11}$$

where $\beta = 1/k_BT$.

Using a second-order cumulant expansion (ref 14, pp 215−216), the spectral broadening function $g(t)$ can be expressed in terms of the frequency-domain correlation function $C''(\omega)$:

$$g(t) = \frac{1}{2\pi}\int_{-\infty}^{\infty}\mathrm{d}\omega\frac{C''(\omega)}{\omega^2}[1 + \coth(\beta\hbar\omega/2)][e^{-i\omega t} + i\omega t - 1] \tag{2.12}$$

with

$$C''(\omega) = -i\int_{-\infty}^{\infty}\mathrm{d}t e^{-i\omega t}\tilde{C}(t) \tag{2.13}$$

and

$$\tilde{C}(t) = -\frac{1}{2\hbar^2}[\langle U(t)U(0)\rho_g\rangle - \langle U(0)U(t)\rho_g\rangle] \tag{2.14}$$

We note that $C''(\omega)$ is in fact the imaginary part of the frequency-domain correlation function $C(\omega)$ with its real part $C'(\omega)$ related to $C''(\omega)$ by

$$C'(\omega) = \coth\frac{\beta\hbar\omega}{2}C''(\omega) \tag{2.15}$$

The function $C''(\omega)$ is a summation of individual contributions from each primary oscillator:

$$C''(\omega) = \sum_j C_j''(\omega) \tag{2.16}$$

where[29]

$$C_j''(\omega) = \frac{2\lambda_j\omega_j^2\omega\gamma_j(\omega)}{\omega^2\gamma_j^2(\omega) + [\omega_j^2 + \omega\Sigma_j(\omega) - \omega^2]^2} \tag{2.17}$$

Here $2\lambda_j$ is the Stokes shift for the jth mode,

$$2\lambda_j = \frac{m_j\omega_j^2 d_j^2}{\hbar} \tag{2.18}$$

$\gamma_j(\omega)$ represents the spectral distribution of the coupling

$$\gamma_j(\omega) = \frac{\pi}{m_j}\sum_n \frac{c_{nj}^2}{2m_n\omega_n^2}[\delta(\omega - \omega_n) + \delta(\omega + \omega_n)] \tag{2.19}$$

and the real part $\Sigma_j(\omega)$ of the self-energy is related to the spectral distribution of the coupling by the Kramers−Kronig relation:[18]

$$\Sigma_j(\omega) = -\frac{1}{\pi}P\,P\int_{-\infty}^{\infty}\mathrm{d}\omega'\frac{\gamma_j(\omega')}{\omega' - \omega} \tag{2.20}$$

where $P\,P$ stands for the Cauchy principal part. This gives

$$\Sigma_j(\omega) = \frac{1}{m_j} P\,P \sum_n \frac{{c_{nj}}^2}{2m_n\omega_n^2}\left[\frac{1}{\omega - \omega_n + i\eta} + \frac{1}{\omega + \omega_n + i\eta}\right], \tag{2.21}$$

where the quantity η is infinitesimal. In general, the coupling of the primary oscillator to the bath is nonlinear. The linear form of the coupling (eq 2.4) is usually justified when the coupling is weak.[19] It implies that the bath friction does not depend on the state of the system in the entire frequency range.

One can also write λ_j as $S_j\hbar\omega_j$ where S_j is the dimensionless Huang−Rhys factor. The value of S_j can vary from much less than unity (weak coupling) to equal to greater than unity (moderate/strong coupling). For example, the molecular ion O_2^- in KBr emits in the visible range of 400−700 nm.[20] The optical center is strongly coupled to the internal vibrational mode of the O_2^- ion with $S_j = 10$ and $\hbar\omega_j = 1000$ cm^{-1}, and at the same time weakly coupled to the phonon modes of KBr with $S_j \sim 1$ and a frequency[20] of less than 200 cm^{-1}. For the B820 complex in the core antenna (LH1) of the purple bacteria, the spectrum is dominated by modes with $S_j \sim 0.5$ and a typical frequency[21] of 100 cm^{-1}. In all of the examples considered below in which one coupled oscillator is assumed, we have taken $S_j = S_1 = 1$.

To facilitate numerical computations, the real and imaginary parts of the line shape function $g(t) = g'(t) + ig''(t)$ can be written in terms of $C''(\omega)$ as follows:

$$g'(t) = \frac{1}{\pi}\int_0^\infty \mathrm{d}\omega\, \frac{1 - \cos(\omega t)}{\omega^2}\coth(\beta\hbar\omega/2)C''(\omega) \tag{2.22}$$

$$g''(t) = \frac{i}{\pi}\int_0^\infty \mathrm{d}\omega \frac{\sin(\omega t) - \omega t}{\omega^2}\mathrm{C}''(\omega) \tag{2.23}$$

These follow from eq 2.12 by applying symmetry considerations.

III. The Correlation Function for the Brownian Oscillator Model

A. Physical Origins of the Correlation Function. The correlation $C''(\omega)$ (eq 2.17) can be obtained rigorously from path integral techniques by tracing over the bath degrees of freedom.[16,19] However, comparisons with the classical Langevin equation provide a better understanding of the spectral distribution function $\gamma_j(\omega)$. The classical Brownian motion is described by the generalized Langevin equation:

$$m_j\frac{\mathrm{d}^2q_j^c(t)}{\mathrm{d}t^2} + m_j\omega_j^2q_j^c(t) + m_j\int_{-\infty}^t \mathrm{d}\tau\gamma_j(t-\tau)\frac{\mathrm{d}q_j^c(t)}{\mathrm{d}t} = f_j(t) + F_j(t) \tag{3.1}$$

Here $q_j^c(t)$ is the c-number displacement of the jth classical oscillator, $\gamma_j(t)$ is the time-dependent damping constant with possible memory effect, $F_j(t)$ is the external driving force, and $f_j(t)$ is the so-called fluctuating force representing the effect of the bath on the jth primary oscillator. The latter is assumed to obey[15,19,14]

$$\langle f_j(t) = 0\rangle \tag{3.2}$$

$$\langle f_j(t)f_k(\tau)\rangle = \delta_{jk}2m_jk_\mathrm{B}T\gamma_j(t-\tau) \tag{3.3}$$

The averages are over stochastic variables. Equation 3.3 is in fact the well-known fluctuation−dissipation theorem which relates relaxation of a weakly perturbed system to the spontaneous fluctuations in the thermal equilibrium. Special cases of the theorem include the Einstein relation between the diffusion constant and the viscosity of a Brownian particle and Nyquist formula for thermal noise in a resistor.

According to the Ehrenfest theorem, the expectation values of a quantum operator obey the classical equations of motion. Therefore, we expect the mean values of the quantum operator $q_j(t)$ to follow eq 3.1. In fact, efforts have been made to generalize the classical Langevin eq 3.1 to the quantum case. The following quantum-mechanical version of the Langevin equation has been obtained[22−24]

$$m_j\frac{\mathrm{d}^2q_j(t)}{\mathrm{d}t^2} + m_j\omega_j^2q_j(t) + m_j\int_{-\infty}^t d\tau\gamma_j(t-\tau)\frac{\mathrm{d}q_j(t)}{\mathrm{d}t} = \xi_j(t) \tag{3.4}$$

where $\xi_j(t)$ is an operator-valued random force with stationary Gaussian statistics. From the fluctuation dissipation theorem, one can obtain in general

$$\langle\xi_j(t)\xi_j(0)\rangle = \frac{\hbar m_j}{\pi}\int_0^\infty \mathrm{d}\omega\omega\gamma_j(\omega)\left(\coth\frac{\hbar\omega\beta}{2}\cos\omega t - i\sin\omega t\right) \tag{3.5}$$

For a discussion on the forms of the fluctuation−dissipation relations for classical and quantum systems, the reader is referred to Cortès et al.[24]

Defining the susceptibility $\alpha_j(\omega)$ to the external perturbation $F_j(\omega)$ through

$$\langle q_j^c(\omega)\rangle = \alpha_j(\omega)F_j(\omega) \tag{3.6}$$

we relate the classical analogue of $C''(\omega)$, $\bar{C}''(\omega)$ to $\alpha_j(\omega)$ by

$$\bar{C}''(\omega) = -\hbar\mathrm{Im}[\alpha_j(\omega)] \tag{3.7}$$

If the dependence of $\gamma_j(\omega)$ on ω is weak, the memory effect of the damping constant γ_j can be neglected. The limit $\gamma_j(t) \rightarrow \delta(t)$ is usually referred to as the Ohmic limit. Below we will first present our calculations of $T^*(\omega)$ for a constant $\gamma_j(\omega) = \gamma_j$ ($\Sigma_j(\omega) = 0$).

B. Characteristic Behavior of the Correlation Functions. We consider first the mode-continuum model, in which it is assumed that the j summations of section II can be replaced by integrals over densities of modes (ref 14, p 221). This suppresses all specific information on oscillator−bath coupling and a model function must therefore be assumed for the correlation function

$$C''(\omega) = 2\lambda\frac{\omega\Lambda}{\omega^2 + \Lambda^2} \tag{3.8}$$

The parameters λ and Λ are assumed temperature-independent, so the only temperature dependence enters through the coth factor in eq 2.12. Figure 1a shows the dependence of $C'(\omega)$ on temperature for a fixed value of Λ and Figure 1b shows the Λ dependence of $C''(\omega)$. Its maxima fall at $\omega = \Lambda$. On this simplified model, $C''(\omega)$ is just the density of oscillators in ω space weighted by $\omega^2/2$ and a continuously distributed coupling strength $S(\omega)$. Remembering this context, one may therefore consider $C''(\omega)$ to be an effective density of states.

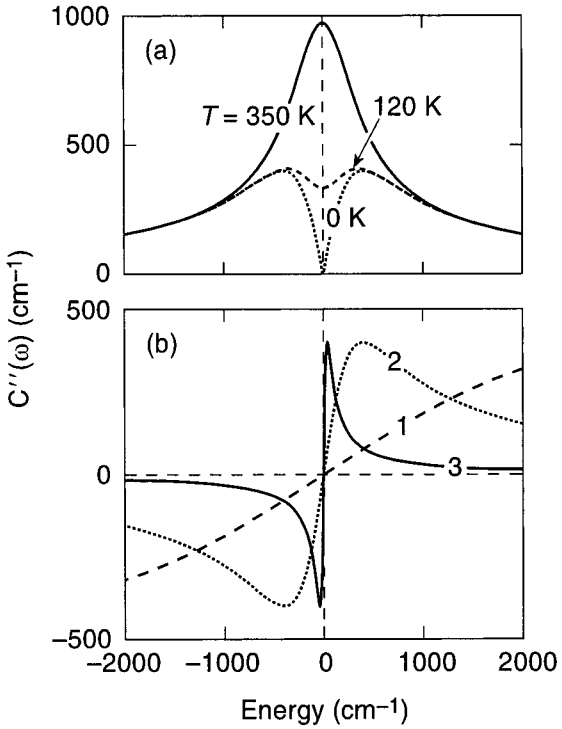

Figure 1. The temperature and damping dependence of $C'(\omega)$ and $C''(\omega)$ on the Brownian oscillator model in the case of a continuum of modes with a width parameter $\Lambda = 400$ cm^{-1} and strength $\lambda = 400$ cm^{-1} ($S = 1$). (a) $C'(\omega)$ increases with temperature, as illustrated for $T = 0$, 120, and 350 K. Values at $\omega = 0$ are given by the limiting expression $4S(\lambda/\Lambda)k_BT$. (b) $C''(\omega)$ for the Brownian oscillator model has no temperature dependence. Shown here are its energy dependence for three different values of the distribution width parameter. Curve 1, $\Lambda = 4000$ cm^{-1}; curve 2, $\Lambda = 400$ cm^{-1}; curve 3, $\Lambda = 40$ cm^{-1}.

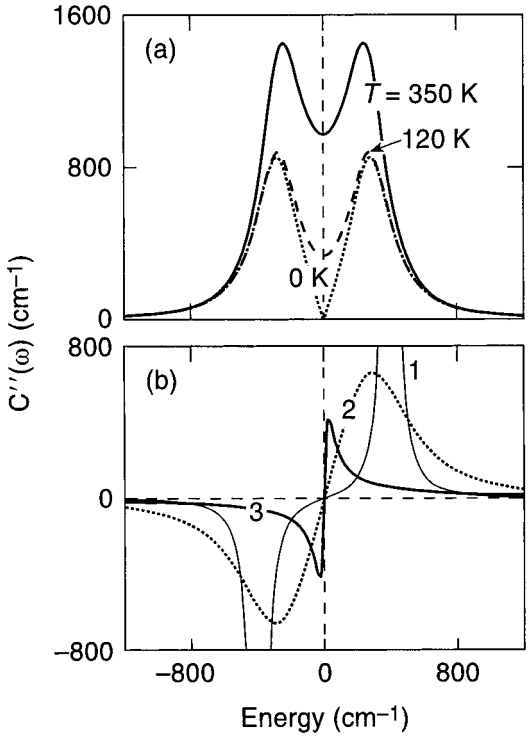

Figure 2. The temperature and damping dependence of $C'(\omega)$ and $C''(\omega)$ on the multimode Brownian oscillator model in the case of one assumed mode of wavenumber $\omega_1 = 400$ cm^{-1}, $\lambda_1 = 400$ cm^{-1} (coupling strength $S_1 = 1$). (a) $C'(\omega)$ increases with temperature. In the case shown, $\gamma_1 = 600$ cm^{-1}. Values at $\omega = 0$ are given by the limiting expression $4S(\lambda/\Lambda)k_BT$. (b) $C''(\omega)$ for the Brownian oscillator model has no temperature dependence. Shown here are its energy dependence for three different values of the damping parameter. Curve 1, $\gamma_1 = 60$ cm^{-1}; curve 2, $\gamma_1 = 600$ cm^{-1}; curve 3, $\gamma_1 = 6000$ cm^{-1}. The resonances in curve 1 are centered at 400 cm^{-1} and have peak values that are 8.6 times the peak values of curve 2.

The multimode Brownian oscillator model, adapted to the case of one oscillator (labeled 1) has the Ohmic-limit correlation function

$$C''(\omega) = \frac{2\lambda_1\omega_1^2\omega\gamma_1}{\omega^2\gamma_1^2 + (\omega_1^2 - \omega^2)^2} \tag{3.9}$$

Figure 2 shows the two parts of $C(\omega)$ in this case with a fixed $\omega_1 = \lambda_1$ and various values of γ_1. The emergence of a strong "density of states peak" at $\omega = \omega_1$ is quite clear in the small damping limit, here represented by $\gamma_1 = 0.1\omega_1$.

In the limit of large γ_1 ($\gamma_1 \gg 2\omega_1$), called the overdamped limit, there is a great resemblance of $C''(\omega)$ on the one-mode model to that in the mode-continuum case (compare Figure 2b, curve 3, with Figure 1b, curve 3]. The connection is not accidental. In this limit, eq 3.9 has nearly the same form as eq 3.8 if we set $\Lambda = \omega_1^2/\gamma_1$. While the two forms are not mathematically equivalent, except for a limited range of frequencies around $\omega \sim \omega_1$, in practice eq 3.8 can be used to simplify calculations in the overdamped case. Appendix A shows that eq 3.8 actually leads to a closed form of $g(t)$.

In both cases shown in Figures 1 and 2, $C'(\omega)$ increases monotonically with temperature for high temperatures. At low temperatures, $C'(\omega)$ has a dip around $\omega = 0$. As temperature is increased, the minimum in $C'(\omega)$ levels off. In the overdamped Brownian oscillator model $C'(\omega)$ clearly dominates at high temperatures.

It is worth noting that a connection between $C''(\omega)$ and either λ or λ_1 exists, given by

$$\lambda = \frac{1}{\pi}\int_0^\infty d\omega \frac{C''(\omega)}{\omega} \tag{3.10}$$

This is very clear for the correlation function eq 3.8, but in the case of eq 3.9 it is helpful to use[25]

$$\int_0^\infty \frac{dx}{ax^4 + bx^2 + c} = \frac{\pi}{2\sqrt{c(b + 2\sqrt{ac})}} \tag{3.11}$$

with $c = 1$, $b = a^2 - 2$. We have used eq 3.10 in testing the accuracy of numerical integration, as discussed in Appendix B.

C. Non-Ohmic Behavior. The bath friction coefficient has so far been set to be constant in all of our calculations. The corresponding spectral density $J_j(\omega)$ defined by

$$J_j(\omega) \equiv \frac{\pi}{2}\sum_n \frac{c_{nj}^2}{m_n\omega_n}\delta(\omega - \omega_n) \tag{3.12}$$

has the form

$$J_j(\omega) = \eta\omega = m_j\gamma_j\omega \tag{3.13}$$

where η is the viscosity coefficient. The spectral density $J_j(\omega)$

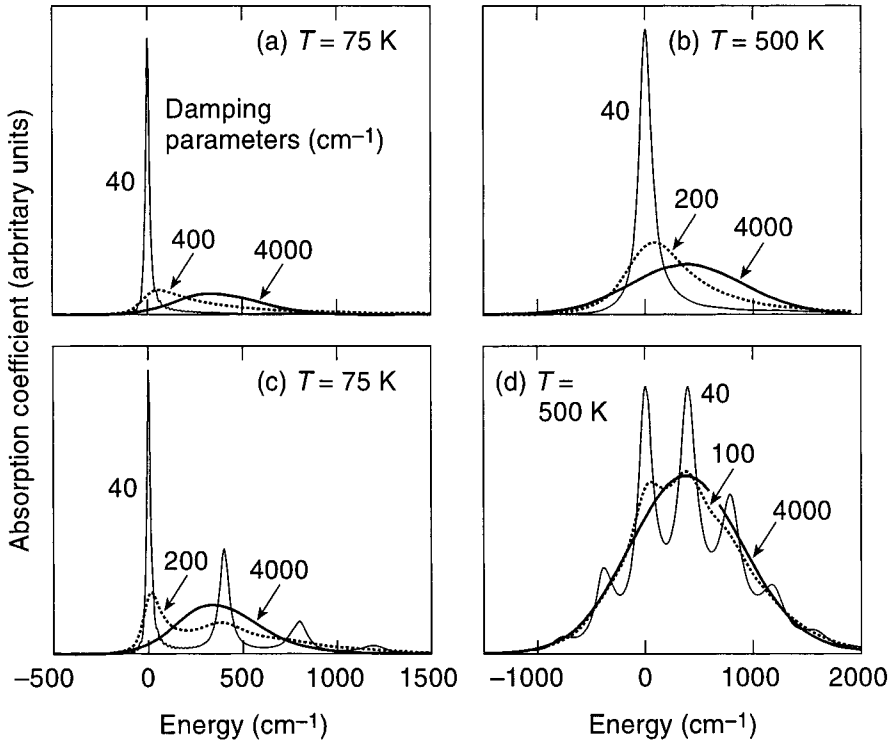

Figure 3. Absorption spectrum predictions of the Brownian oscillator model. (a, b) The mode continuum model with density-of-states parameters $\Lambda = 4000$, 400, and 40 cm^{-1}, at 75 K and 500 K, as marked. (c, d) The multimode model with one mode having parameters of $\omega_1 = 400$ cm^{-1} and $\gamma_1 = 40$, 400, and 4000 cm^{-1}, again at the same two temperatures. Ordinate in arbitrary units.

is also related to the damping kernel $\gamma(t)$ by

$$J_j(\omega) = m_j\omega\int_0^\infty \gamma(t)\cos(\omega t)\,\mathrm{d}t \tag{3.14}$$

Therefore, for Ohmic dissipation eq 3.13 follows. In reality, the spectral density $J_j(\omega)$ falls off for large ω, reflecting the microscopic memory time scales for inertia effects in the bath. Therefore, a realistic damping coefficient $\gamma_j(\omega)$ will not be frequency-independent. One usually assumes the spectral density function behaves as ω^s with $s > 0$ at low frequencies with a high-frequency cutoff ω_c. The $s = 1$ case is the Ohmic bath, and the $s < 1$ and $s > 1$ cases are named sub-Ohmic and super-Ohmic baths, respectively.

Consider pure liquid water as an example. Molecular dynamics has been applied to water to compute the velocity spectrum which reveals the density of normal modes of a solvent.[26] It is found that the velocity spectrum of pure liquid water has a low-frequency band near 50 cm^{-1} that extends to several hundred wavenumbers corresponding to hindered translation, a broad region around 1300 cm^{-1} corresponding to libration, a region around 1700 cm^{-1} due to bending modes, and a high-frequency region near 3700 cm^{-1} due to stretching modes of water molecules. Because solvent motion is responsible for friction, corresponding features are found in the friction spectrum, which displays a strong frequency dependence.[27]

For frequency-dependent damping, it is convenient to define $\bar{\gamma}_j(\omega)$ through analytical continuation of the Laplace transform of the damping kernel $\gamma_j(t)$:

$$\bar{\gamma}_j(\omega) \equiv \hat{\gamma}_j(s = -i\omega) \tag{3.15}$$

For example, the Drude-regularized damping kernel $\gamma_j(t)$ has a memory time $\tau_D = 1/\omega_D$:

$$\gamma_j(t) = \gamma\omega_D \exp(-\omega_D t) \tag{3.16}$$

Then one obtains

$$\hat{\gamma}_j(s) = \frac{\gamma\omega_D}{\omega_D + s} \tag{3.17}$$

By analytical continuation, $\tilde{\gamma}_j(\omega)$ is no longer real. In fact $\Sigma_j(\omega)$ in section II is equivalent to the imaginary part of $\tilde{\gamma}_j(\omega)$ defined by analytical continuation of $\gamma_j(s)$:

$$\gamma_j(\omega) = \mathrm{Re}\tilde{\gamma}_j(\omega) \tag{3.18}$$

$$\Sigma_j(\omega) = \mathrm{Im}\tilde{\gamma}_j(\omega) \tag{3.19}$$

From eq 3.17, the imaginary part of γ_j is smaller by a factor of ω/ω_D than its real part

$$\tilde{\gamma}_j(\omega) = \frac{\gamma\omega_D}{\omega_D^2 + \omega^2}(\omega_D + i\omega) \tag{3.20}$$

Such a model for non-Ohmic dissipation is also used recently in modeling quantum control of dissipative systems.[28] Finally we point out that eq 3.10 is again satisfied for the damping kernel eqs 3.18 and 3.19, with a memory time τ_D, as for the Ohmic dissipation:

$$\int_0^\infty \frac{\gamma_j(x)\,\mathrm{d}x}{x^2\gamma_j(x) + [1 + x\Sigma_j(x) - x^2]^2} = \frac{\pi}{2} \tag{3.21}$$

IV. The KS Temperature in Steady-State Spectra

As an illustration of the application of the Brownian oscillator model, in Figure 3 we show the absorption line shapes for the continuum model (a, b) and for a mildly overdamped Brownian oscillator model (c, d). Each is presented for two temperatures sufficiently different to produce qualitatively distinct spectra.

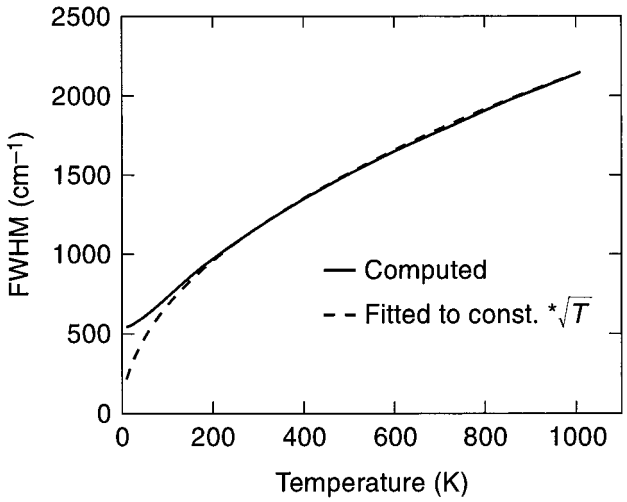

Figure 4. Full width at half-maximum (fwhm) of the absorption line shapes as a function of temperature. The multimode model is used with parameters $\omega_1 = 600$ cm^{-1}, $\gamma_1 = 4000$ cm^{-1}, and $\lambda_1 = 600$ cm^{-1}. The solid line is a superposition of two computed cases, one for Ohmic damping and one for non-Ohmic ($\omega_D = 6000$ cm^{-1}). The dashed line is a fit to $67.348\sqrt{T}$.

The intermediate damping parameter is varied among the pictures in order to make the intermediate case interesting. (A value of 400 did not produce anything distinctive in cases b, c, and d.) The two models make similar predictions at large γ_1 (small Λ) because, as explained above, the correlation function (eq 3.8) is then approximately of the same form as that of the multimode model, with $\Lambda = \omega_1^2/\gamma_1$. Our parameters have been chosen to satisfy this. At the same time, the line shape approaches a Gaussian. From Figure 3, it is readily appreciated that the effective density of states represented by $C''(\omega)$ is appearing as a convolved sideband on narrow spectral features, and that any narrow features are washed out by either large damping or high temperature.

In Figure 4, the fwhm (full-width at half-maximum) is plotted as a function of temperature T for a mildly overdamped case ($\gamma_1/2\omega_1 = 3.33$). The line width grows with the temperature. The solid line is a superposition of computed cases, one for Ohmic damping and one for non-Ohmic ($\omega_D = 6000$ cm^{-1}), illustrating the independence of fwhm on this parameter. The dashed line is a fit to $67.348\sqrt{T}$, illustrating the usual $\sqrt{T}$ dependence at $T \geq \hbar\omega_1/2$.

In Figure 5, complete results are shown for absorption profile, emission profile, KS function F, and KS spectral temperature T^*. The ambient temperature is 300 K, and parameters are chosen to mimic the principal line of a typical room-temperature dye molecule spectrum. What is seen here is typical of a series of calculations. It was found that the expected result $T^*(\omega) = T$ could be realized only at the cost of numerical adjustments. These adjustments were sometimes capable of producing a completely flat $T^*(\omega)$ curve, but departures and divergences outside the Stokes region were very common. These divergences (near ± 1500 cm^{-1} in Figure 5) naturally should not be present in such an equilibrated case and they appear to be artifacts of the numerical calculation, as discussed in Appendix B. Despite these difficulties, the computed T^* in the central Stokes region (~ -500 to $+500$ cm^{-1}) very closely matches the ambient temperature.

We now turn our attention to underdamped Brownian oscillators and the results shown in Figures 6 and 7. To elaborate a bit further on the case of underdamped oscillators at low temperatures, consider the completely undamped oscillators at

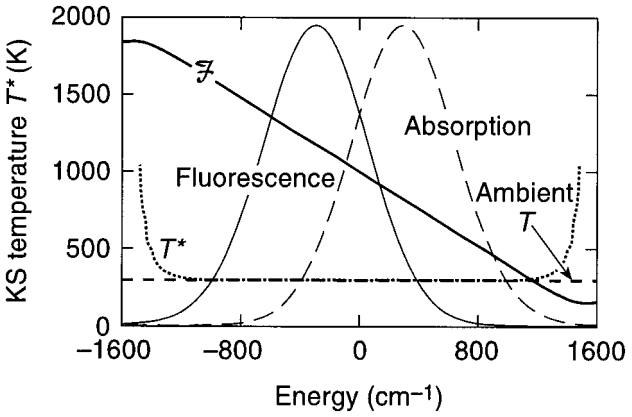

Figure 5. Absorption, fluorescence, and $T^*(\omega)$ spectra for an overdamped case of the multimode oscillator model, parameters of the one mode being $\gamma_1 = 6000$ cm^{-1}, $\lambda_1 = \omega_1 = 300$ cm^{-1}, and $T = 300$ K. Here the parameter $\Lambda_1 = \omega_1^2/\gamma_1 = 0.05\lambda_1 = 15$ cm^{-1}. Energy is measured from the 0−0 level. Absorption, fluorescence, and F are on arbitrary scales.

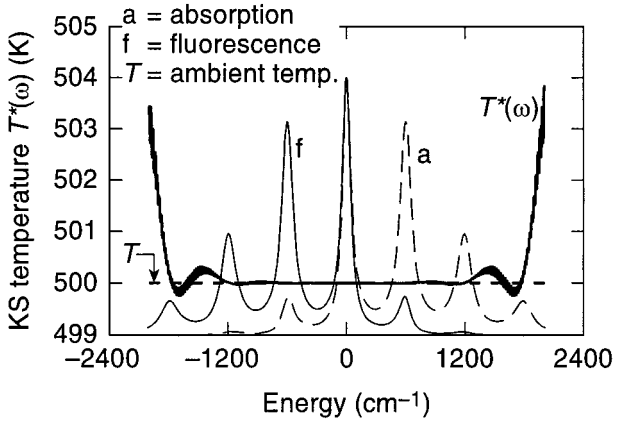

Figure 6. Absorption and fluorescence line shapes plotted (arbitrary scale) with the spectral temperature $T^*(\omega)$ for an underdamped and Ohmic case with $\gamma_1 = 40$ cm^{-1}, $\lambda_1 = \omega_1 = 600$ cm^{-1}, and $T = 500$ K. Note that the spectral temperature is closely equal to the ambient despite the usual singularities that are becoming evident near ± 2000 cm^{-1}. Energy is measured from the 0−0 level.

zero temperature with only the zero number state occupied in the ground-state manifold. The weak-coupling limit at zero temperature has an absorption line shape given by[13,14]

$$\sum_{n=-\infty}^{\infty} \frac{e^{-S_j} S_j^n}{n!} \delta(\omega - \omega_{eg} + n\omega_j) \tag{4.1}$$

where $S_j = \lambda_j/\omega_j$ is again the Huang−Rhys factor. As the temperature is increased, higher number states in the ground-state manifold are occupied. The summation in eq 4.1 is replaced by[13]

$$e^{-S_j(2\bar{n}+1)} \sum_{n=-\infty}^{\infty} \exp\left(\frac{n\beta\hbar\omega_j}{2}\right) I_n[2S_j(2\bar{n}+1)] \delta(\omega - \omega_{eg} + n\omega_j) \tag{4.2}$$

where $\bar{n} = 1/[\exp(\beta\hbar\omega j) - 1]$, $I_n(x)$ is the modified Bessel function, and the sum over n is extended to negative n as compared to eq 4.1. If damping is further added, the delta function peaks in eq 4.2 acquire a finite width. Thus the main features in Figures 6 and 7 are obtained. The envelope of the phonon sidebands (with index n) represents the effect of adding

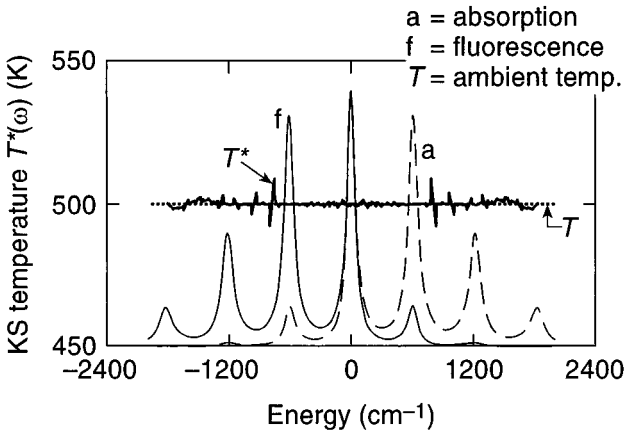

Figure 7. Absorption and fluorescence line shapes plotted (arbitrary scale) with the spectral temperature $T^*(\omega)$ for an underdamped non-Ohmic case with $\gamma_1 = 40$ cm^{-1}, $\lambda_1 = \omega_1 = 600$ cm^{-1}, $\omega_D = 600$ cm^{-1} and $T = 500$ K. In this best case the extreme sensitivity to numerical computation is illustrated. Comparing the temperature scale with that of Figure 6, this is seen to be much less accurate. Nonetheless, the T^* excursions from ambient are similar and have singularities near ±2000 cm^{-1}. Energy is measured from the 0−0 level.

a finite width proportional to n which smears out the structure at large phonon numbers.

Included with the line profiles in Figures 6 and 7 are the computed spectral temperatures $T^*(\omega)$. Despite the rich structure in the absorption and emission, we have obtained a rather flat $T^*(\omega)$ in the Stokes region where both $\sigma_{BO}(\omega)$ and $I_{BO}(\omega)$ are at a significant fraction of their maximum value. In Figure 6, the high-frequency oscillations of $T^*(\omega)$ are a numerical artifact, but we call attention to the temperature scale. This is one of the most successful cases in terms of reproducing the KS theoretical result.

We calculate the spectral temperature formally in the same manner as we did for the Ohmic case. In Figure 7, we display $T^*(\omega)$ for a non-Ohmic bath with $\omega_D = \omega_1$. The spectral temperature $T^*(\omega)$ still equals the ambient temperature T and is rather flat in the Stokes region. The numerical problems were a bit more severe in this case, and the smoothing obviously required was deliberately not done in order to illustrate this. It appears that as long as a relaxed fluorescence spectrum is used for $T^*(\omega)$, regardless of the process by which the relaxation occurs and the time it might take, we can expect to obtain $T^* = T$. In practice, steady-state fluorescence spectra are equivalent to the average spectrum seen over the lifetime of the excited state. We now turn to the time-resolved fluorescence case where it is a priori the case that equilibrium has not occurred.

V. Time-Resolved Fluorescence

A. Basis of a Time-Dependent Theory. The KS theory will be extended to the time-resolved case by a simple modification of eq 1.2, as follows:[31]

$$T^*(\omega,t) = -\left[\frac{k_B}{\hbar}\frac{d}{d\omega}\ln\frac{I(\omega,t)}{\sigma(\omega)}\right]^{-1} \tag{5.1}$$

Assuming no time dependence in the absorption coefficient may limit $T^*(\omega,t)$ to cases in which ground-state depletion is negligible. The normal absorption spectrum is the natural reference spectrum for the formalism because of its important role in relating microstate transition probabilities between the excited and ground manifolds. It is important to note, however, that the application of eq 5.1 to single manifolds is still limited to cases in which the excited state is not kinetically coupled to other states.

As pointed out earlier,[31] a somewhat more general time-dependent Kennard−Stepanov function F could be constructed by including time dependence in the absorption coefficient, ensuring that the set of fluorescence transitions would precisely match the corresponding absorption transitions. It is not clear that such a broader definition would be useful. If the absorption coefficient is significantly time dependent, then the experiment has reached a nonlinear regime and more than one pair of electronic levels may be involved in each of the spectra, a degree of complication unwelcome at this early stage of the theory. Furthermore, it is unlikely that simultaneous fluorescence and pump−probe measurements will be available for the same sample. Only in the context of demonstrating the equilibrium KS relation is it essential that the fluorescent and absorptive transitions match precisely; maintaining the ground-state absorption as a reference spectrum is reasonable in the absence of a precise non-equilibrium theory. We therefore do maintain it and caution that our time-dependent temperature analysis should be applied only in nonsaturating excitation conditions.

B. Formalism. To calculate the time-resolved fluorescence, we use the third-order response functions. At third order in the radiation field, the polarization is given by

$$P^{(3)}(\mathbf{r},t) = \int_0^\infty dt_3 \int_0^\infty dt_2 \int_0^\infty dt_1 S^{(3)}(t_3,t_2,t_1) E(\mathbf{r},t-t_1)E(\mathbf{r},t-t_2-t_1)E(\mathbf{r},t-t_3-t_2-t_1) \tag{5.2}$$

Here the response function $S^{(3)}(t_3,t_2,t_1)$ is a sum of four terms (ref 14, p 122)

$$S^{(3)}(t_3,t_2,t_1) = (i/\hbar)^3\theta(t_1)\theta(t_2)\theta(t_3)\sum_{\alpha=1}^{4}[R_\alpha(t_3,t_2,t_1) - R_\alpha^*(t_3,t_2,t_1)] \tag{5.3}$$

with

$$R_1(t_3,t_2,t_1) = \exp[-g(t_1) - g^*(t_2) - g^*(t_3) + g(t_1+t_2) + g^*(t_2+t_3) - g(t_1+t_2+t_3)]$$

$$R_2(t_3,t_2,t_1) = \exp[-g^*(t_1) + g(t_2) - g^*(t_3) - g^*(t_1+t_2) - g(t_2+t_3) + g^*(t_1+t_2+t_3)]$$

$$R_3(t_3,t_2,t_1) = \exp[-g^*(t_1) + g^*(t_2) - g^*(t_3) - g^*(t_1+t_2) - g^*(t_2+t_3) + g^*(t_1+t_2+t_3)]$$

$$R_4(t_3,t_2,t_1) = \exp[-g(t_1) - g(t_2) - g(t_3) + g(t_1+t_2) + g(t_2+t_3) - g(t_1+t_2+t_3)] \tag{5.4}$$

These results are exact for the Brownian oscillator model. For anharmonic systems such as a chromophore coupled to a spin bath (the TLS model),[29,30] third-order responses cannot in general be expressed in terms of linear response functions. In the weak-coupling limit, eqs 5.4 are found to be obeyed to the second-order in the cumulant expansion in the TLS model, and higher order corrections have been derived.[29]

Assume that the full electric field $\hat{E}(t)$, including the classical excitation field and the emitting field, takes the form

$$\hat{E}(t) = 2E_1(t)\cos(\omega_{ex}t) + \hat{E}_2 + \hat{E}_2^\dagger \tag{5.5}$$

with

$$\hat{E}_2 = -iE_2c_2\exp(-i\omega t) \tag{5.6}$$

where c_2 destroys a photon with frequency ω. The time-resolved fluorescence $S(\omega_{ex},\omega,t)$ is given by the expectation value of the commutator

$$\hat{S} = (i/\hbar)[\hat{H}(t),c_2^{\dagger}c_2] \tag{5.7}$$

which represents the time derivative of the photon numbers. To fourth order in the radiation−matter coupling strength, $S(\omega_{ex},\omega,t)$ is calculated from

$$S(\omega_{ex},\omega,t) = \frac{1}{2\pi}\mathrm{Re}\int_0^{\infty}dt_1\int_0^{\infty}dt_3 R_1(t_3,t,t_1)\exp[-\omega^2 t_1^2 + i(\omega_{ex} - \omega_{eg}{}^0)t_1 + i(\omega - \omega_{eg}{}^0)t_3] \tag{5.8}$$

provided that the temporal envelope of the excitation pulse has a Gaussian form:

$$E_1(t) = E_1\exp(-\omega^2 t^2) \tag{5.9}$$

In the case when the pump pulse is narrow enough to be approximated by a delta function (impulse excitation), the time-resolved fluorescence is independent of ω_{ex}:

$$S(\omega_{ex},\omega,t) = \frac{1}{2\pi}\mathrm{Re}\int_0^{\infty}dt_3 R_1(t_3,t,0)\exp[i(\omega - \omega_{eg}^0)t_3] \tag{5.10}$$

Consider the overdamped Brownian oscillator model at high temperatures as an example. The line shape function $g(t)$ can be approximated by

$$g(t) = \frac{2\lambda}{\hbar\beta\Lambda^2}(e^{-\Lambda t} + \Lambda t - 1) - i\frac{\lambda}{\Lambda}(e^{-\Lambda t} + \Lambda t - 1) \tag{5.11}$$

with its imaginary part much smaller that its real part. Then the third-order response function $R_1(t_3,t,0)$ is simply

$$R_1(t_3,t,0) = \exp[i2\mathrm{Im}[g(t) - g(t + t_3)] - g^*(t_3)] \tag{5.12}$$

Carrying out the Fourier transformation with respect to t_3, one can easily see the time evolution of the dynamic Stokes shift. In particular, noticing that

$$\lim_{t\to\infty}\mathrm{Im}[g(t)] = \lambda t \tag{5.13}$$

the relaxed fluorescence is recovered as $t \to \infty$:

$$S(\omega_{ex},\omega,t = \infty) = I(\omega) \tag{5.14}$$

At $t = 0$, the fluorescence profile equals the absorption profile

$$S(\omega_{ex},\omega,t = 0) = \sigma(\omega) \tag{5.15}$$

In fact eqs 5.14 and 5.15 hold for all forms of $g(t)$ because the asymptotic behavior of $g(t)$ in eq 5.13 is easily derived from eq 2.23.

The effect of excited-state lifetime can be taken into account by adding an imaginary frequency to ω:

$$S(\omega_{ex},\omega + i/\tau_e,t) = \frac{1}{2\pi}\mathrm{Re}\int_0^{\infty}dt_1\int_0^{\infty}dt_3 R_1(t_3,t,t_1)\exp[-\omega^2 t_1^2 - t_3/\tau_e + i(\omega_{ex} - \omega_{eg}^0)t_1 + i(\omega - \omega_{eg}^0)t_3] \tag{5.16}$$

In the case of a delta-function excitation pulse,

$$S(\omega_{ex},\omega + i/\tau_e,t) = \int_{-\infty}^{\infty}dt_3 R_1(t_3,t,0)\exp[-t_3/\tau_e + i(\omega - \omega_{eg}^0)t_3] \tag{5.17}$$

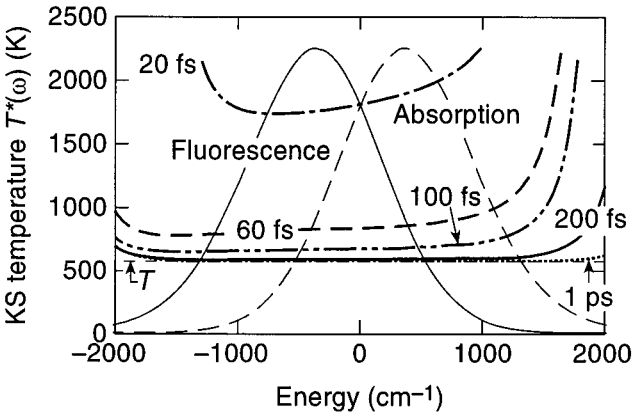

Figure 8. $T^*(\omega)$ derived from the steady-state absorption spectrum and the time-resolved fluorescence spectra (at the times shown on the diagram). The horizontal line is the ambient temperature, chosen here to correspond to the value of $\lambda_1 = \omega_1 = 400$ cm^{-1}. Other parameters are $\gamma_1 = 1600$ cm^{-1} and $\omega_D = 40{,}000$ cm^{-1}. The relatively large value of ω_D ensures near-Ohmic damping. The divergences in $T^*(\omega)$ are discussed in the text. It is believed that the temperature values in the central Stokes region (−500 to 500 cm^{-1}) are the most significant. Energy is measured from the 0−0 level.

C. Predicted Time-Dependent Spectra. Figure 8 shows the spectral temperature associated with emission from a mildly overdamped Ohmic system after excitation with a $\delta(t)$ pulse. The parameters are shown in the caption. The temperatures at the center of the energy range ($\omega = \omega_{eg}{}^0$) are undoubtedly the most meaningful, since the numerical difficulties found in the steady-state case are present and sometimes amplified here (see Appendix B). These temperatures exhibit a complex decay that is at least triphasic, with time constants 44.6 fs, 12 fs, and ultrashort.

Because of the assumed spectrally broad excitation, the fluorescence associated with the temperature series is broad and its width changes little, unlike the case of narrow excitation treated earlier.[31] The shapes are nearly Gaussian. The fluorescence exhibits a time-dependent Stokes shift in which the peak energy can be fit well to the expression $\Delta\omega_{SS} = 725.6[1 - \exp(-t/51.2)]$ cm^{-1}, where t is in fs. The rms deviation of this fit is 15 cm^{-1}, most contributions coming from values at small times. This empirically determined time dependence is quite reasonable, because it is of the form known exactly in the high-temperature overdamped limit,[32] where the decay constant is Λ ($= \omega_1{}^2/\gamma_1$ in our case) = 100 cm^{-1} = 1/(53.1 fs).

Figure 9 shows the effect of non-Ohmic dissipation with conditions otherwise the same as in Figure 8. There are three significant differences from the Ohmic case. First, the shapes of the temperature curves $T^*(\omega,t)$ are radically altered; second, the terminal Stokes shift is considerably smaller; and third, the Stokes shift is not monotonically rising. There is a brief pause at approximately 30 fs, as shown in Figure 10. Smoothing this pause, the Stokes shift can again be fitted with the reasonable form $\Delta\omega_{SS} = 653[1 - \exp(-t/50.1)]$ cm^{-1}. Both terminal Stokes shifts are smaller than that which would occur in the overdamped high-temperature limit, $2\lambda = 800$ cm^{-1}.

D. Limitations. Attempts to extend the calculations to the underdamped oscillator failed because $I(\omega,t)$ itself began to develop negative values whose magnitude was much too large to be finessed with the methods sketched in Appendix B. As an example, for an Ohmic case with $\gamma_1 = 100$ and $\omega_1 = 100$ cm^{-1}, a strong negative feature appears at 30 fs at $\omega = \omega_{eg}^0 +$ 400 cm^{-1}, preceded by a rapid drop in the positive peak originally appearing at that energy. No similar phenomenon

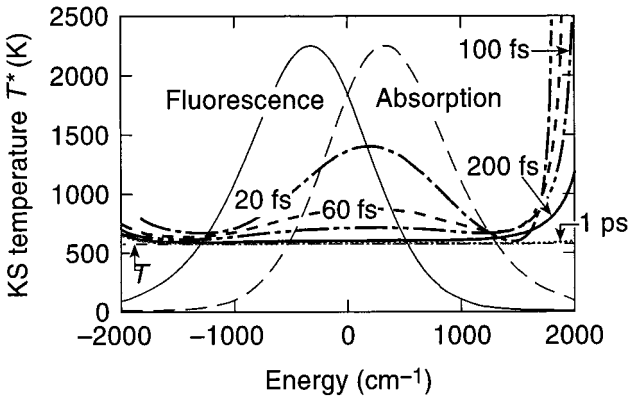

Figure 9. Same as Figure 8, with $\omega_D = 400$ cm^{-1}. In this non-Ohmic case the drop in temperature in the central Stokes region appears to be faster, although the Stokes shift (not shown) has virtually the same time constant as in the Ohmic case.

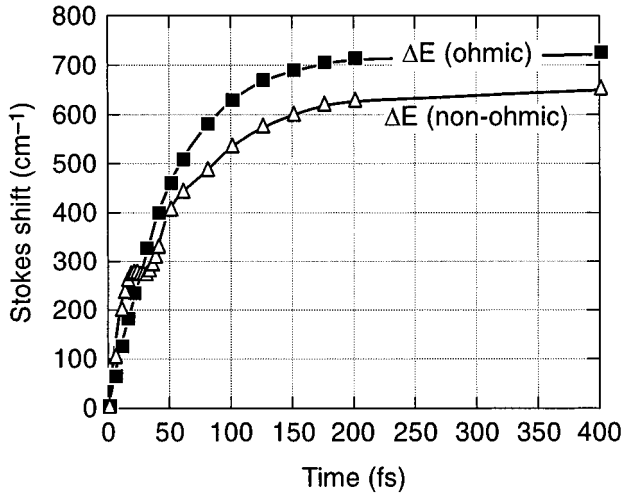

Figure 10. After pulse excitation, the emission peak shifts toward the red. In the Ohmic-damping case corresponding to Figure 8 (shown with solid squares), the computed rise is monotonic. In the non-Ohmic-damping case corresponding to Figure 9 (shown with triangles), a pause interrupts the rise at approximately 20 fs.

occurs on the low energy side. The problem could not be traced to numerical accuracy and undoubtedly represents the failure of the present formalism to produce strictly observable signals. Using eq 5.7 generates a "bare" signal[33,34] that is not restricted to positive values. At small damping the importance of using appropriate gating functions to produce a physically observable signal has become paramount. An extension of our work in this direction is beyond the scope of the paper but represents a possibly interesting avenue for future model calculations.

VI. Summary

The Brownian oscillator model has been widely applied to solvent−solute systems. However, the absorption line shape and the relaxed fluorescence line shape of the model have not heretofore been examined in the framework of KS theory. Here we show in a numerical context that the KS relation holds regardless of system-bath coupling strength and bath memory effects if absorption and fluorescence line profiles follow eqs 2.5. We also find that the KS temperature behaves qualitatively in the same manner as a real temperature of the excited manifold, being large over the Stokes region at early times after excitation and dropping to ambient after characteristic relaxation times.

Acknowledgment. The authors thank S. Mukamel for very enlightening discussions, and V. Chernyak, J. H. Eberly, K. Lindenberg, and E. V. Tsiper for useful conversations. Research was supported in part by National Science Foundation grant PHY-94-15583 (ZK, Rochester Theory Center) and by U.S. Department of Agriculture NRICGO grant 95-37306-2014 (RK).

Appendix A. Closed Expressions for the Line Shape Function for the Overdamped Brownian Oscillator Spectral Density

For future reference it is useful to note that the line shape function $g(t)$ for the Brownian oscillator model may be written in closed form in the case of the simplified correlation function of eq 3.9. Following the notation and development of Mukamel (ref 14, pp 216−217), $g(t)$ can be written

$$g(t) = \Delta^2 \int_0^t d\tau_2 \int_0^{\tau_2} d\tau_1 M'(\tau_1) - i\lambda \int_0^t d\tau [1 - M''(\tau)] \quad \text{(A.1)}$$

$$M'(t) = \frac{1}{\pi\Delta^2} \int_0^\infty d\omega C''(\omega) \coth\frac{\beta\hbar\omega}{2} \cos\omega t \quad \text{(A.2)}$$

$$M''(t) = \frac{1}{\pi\lambda} \int_0^\infty d\omega \frac{C''(\omega)}{\omega} \cos\omega t \quad \text{(A.3)}$$

$$\Delta^2 = \frac{1}{\pi} \int_0^\infty d\omega C''(\omega) \coth\frac{\beta\hbar\omega}{2} \quad \text{(A.4)}$$

$$\lambda = \frac{1}{\pi} \int_0^\infty d\omega \frac{C''(\omega)}{\omega} \quad \text{(A.5)}$$

The meromorphic function $\coth(\beta\hbar\omega/2)$ may be expanded as a summation over its poles which are the Matsubara frequencies for bosons:[13]

$$\coth\frac{\beta\hbar\omega}{2} = \frac{2}{\hbar\beta} \sum_n \frac{1}{i\nu_n - \omega} \quad \text{(A.6)}$$

with

$$\nu_n = \frac{2n\pi}{\hbar\beta} \quad n = 0, \pm1, \pm2, \ldots \quad \text{(A.7)}$$

This allows representing $M'(t)$ and Δ^2 in terms of the Matsubara frequencies ν_n by means of contour integrations

$$\Delta^2 = \lambda\Lambda \cot\frac{\hbar\beta\lambda}{2} + \frac{4\lambda\Lambda}{\hbar\beta} \sum_n \frac{\nu_n}{\nu_n^2 - \Lambda^2} \quad \text{(A.8)}$$

$$M'(t) = \frac{1}{\Delta^2}\left(\lambda\Lambda \cot\frac{\hbar\beta\lambda}{2} e^{-\Lambda t} + \frac{4\lambda\Lambda}{\hbar\beta} \sum_n \frac{\nu_n e^{-\nu_n t}}{\nu_n^2 - \Lambda^2}\right) \quad \text{(A.9)}$$

Contour integrations also yield $M''(t)$:

$$M''(t) = e^{-\Lambda t} \quad \text{(A.10)}$$

and eq A.5 reduces to an identity. The line shape function $g(t)$ is therefore obtained from eq A.1 as

$$g(t) = g'(t) + ig''(t) \quad \text{(A.11)}$$

$$g'(t) = \frac{\lambda}{\Lambda}\cot\frac{\hbar\beta\Lambda}{2}(e^{-\Lambda t} + \Lambda t - 1) + \frac{4\lambda\Lambda}{\hbar\beta}\sum_{n=1}^{\infty}\frac{e^{-\nu_n t} + \nu_n - 1}{\nu_n(\nu_n^2 - \Lambda^2)} \quad \text{(A.12)}$$

$$g''(t) = \frac{\lambda}{\Lambda}\cot\frac{\pi\beta\Lambda}{2}(e^{-\Lambda t} + \Lambda t - 1) \quad \text{(A.13)}$$

The summation in eq A.12 can be carried out and results are expressed in terms of special functions:[29]

$$g'(t) = \frac{\lambda}{\Lambda}\cot\frac{\hbar\beta\Lambda}{2}(e^{-\Lambda t} + \Lambda t - 1) + \frac{\lambda}{\pi\Lambda}\left[2\gamma_E + 2\log(1 - e^{-\nu t}) + e^{-\nu t}\Phi\left(e^{-\nu t},1,\frac{\nu - \Lambda}{\nu}\right) + e^{-\nu t}\Phi\left(e^{-\nu t},1,\frac{\nu - \Lambda}{\nu}\right) + (1 - \Lambda t)\Psi^{[0]}\left(\frac{\nu - \Lambda}{\nu}\right) + (1 + \Lambda t)\Psi^{[0]}\left(\frac{\nu + \Lambda}{\nu}\right)\right] \quad \text{(A.14)}$$

where $\nu = 2\pi/\hbar\beta$, γ_E is Euler's constant ($\sim$0.577216), $\Phi(z,s,a)$ is the Lerch transcendent,[35] and $\Psi^{[n]}(z)$ is the digamma function.[35,36]

Appendix B. Numerical Methods and Accuracy

Evaluation of Integrals and Basic Accuracy Tests. The computational pathway is to perform the quadratures necessary for $C''(\omega)$, $g(t)$, and the spectra, in that order. Each was done with the simplest trapezoidal method. The aliases of "infinity" in each integral were validated by inspecting the range of the integrands and minimizing the effect of varying their values. Integrations were terminated when the contribution of the last bin would have been less than a fraction δ of the accumulated value, where δ was decreased until it had no more effect, often to as small as 10^{-10}. Similarly, the integration interval was varied, the number of bins lying typically between 4000 and 20 000.

In the case of $C''(\omega)$, an automatic test was possible through eq 3.10, which connects the model parameters to λ_j. In all of our examples, parameter values such that $\lambda_j = \omega_j$ were used. Figure 1 provides an example: since the integrand of eq 3.10 contains $1/\omega$, the range 0−4000 cm^{-1} would be adequate for curve 3, but certainly not for curve 1 and probably not for curve 2. The $C''(\omega)$ test was satisfied to within 1% in all cases. Subsequent integrands that contain $C''(\omega)$ contain a factor $1/\omega^2$. Therefore the low-frequency contributions to the integral are most relevant, and the cutoff produces a much better than 1% accuracy.

The complexity introduced by a sequence of three approximate integrations makes a precise numerical accuracy estimate rather difficult. With the exception of certain time-resolved emission cases to be discussed below, the predicted line shapes themselves present a very reasonable picture on physical grounds. However, processing the spectra by the KS formalism brings out some interesting problems.

Anomalies in the KS Function. In computing Brownian oscillator model steady-state spectra, one makes the assumption that emitting states are at thermal equilibrium in the excited manifold. It follows that $F(\omega)$ should be linear and $T^*(\omega)$ should be equal to ambient T at all ω. This is hardly ever fully the case, and the results of a raw calculation are frequently discouraging (Figure 11a). Attempts to remove divergences, which sometimes occur in many places, by increasing all accuracy parameters to the severest practical limits failed. It

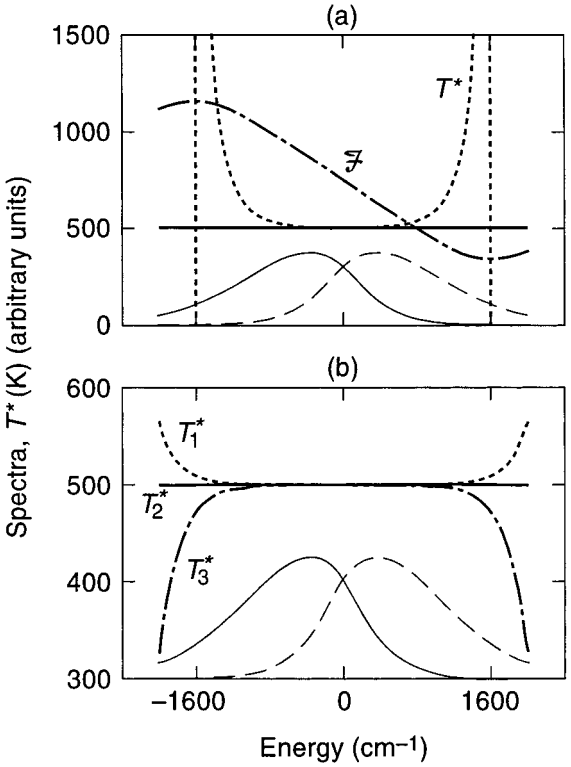

Figure 11. An example of divergences occurring in $T^*(\omega)$ despite reasonable appearance of spectra. In this Ohmic case $\lambda_1 = \omega_1 = 600$ cm^{-1}, $\gamma_1 = 400$ cm^{-1}, and $T = 500$ K. Absorption and emission profiles are shown in the usual way. (a) KS temperature derived directly from computed spectra. The vertical lines are a true representation of T^* as it drops to negative values, passing through singularities resulting from the extrema in F. (b) KS temperatures computed with constant offsets. In units of the limiting value of the absorption spectrum at the lowest energy, the offsets are 0.920, 0.9259, and 0.940 (T_1^*, T_2^*, T_3^*, respectively). For these cases, F is omitted because it is virtually a straight line. Figure 11a corresponds to an offset of 0.00.

was noticed, however, that all the spectra had a small and frequency-independent offset from zero in regions where they were expected to be negligible, i.e., on the very low energy side of absorption bands and the high energy side of emission bands. This offset was little affected by all of the accuracy adjustments and appeared therefore to be an intrinsic difficulty with the trapezoidal integration. Subtraction of a constant offset, a single parameter applied to both fluorescence and emission, dramatically changed the singularities and in some cases completely removed them. This is illustrated in Figure 11b, which is a plot of the KS temperature for the case of Figure 11a but including the offsets. It is an empirical patch the need for which and the success of which are not currently explained. After using this empirical patch, in almost every case within a range $\pm\lambda$ around the zero−zero energy $T^*(\omega)$ can be made closely equal to T, as seen in Figures 6 and 7. The patch is of purely computational interest, because the associated spectra are unchanged except for the small offset.

The Time-Resolved Case. In an explicitly nonequilibrated emitting system, the standard KS relation cannot apply, but as argued in section V and earlier,[31] it may be used to "project out" the departures from equilibrium. There must be no saturation and no competing processes such as transfer to another excited electronic manifold. Given all this, the connection with the normal KS calculation is clearly that as the emission spectrum approaches the steady-state spectrum, $T^*(\omega)$ should flatten out. Since the time-resolved calculation here used the same algorithms as our steady-state, the same offset anomalies

and therefore similar $T^*(\omega)$ anomalies were found. To prevent too many unrelated fitting parameters, we found the best offset by minimizing the mean square deviation of $T^*(\omega)$ from T in the Stokes region for the emission computed at the longest time and used the same offset for all spectra. This generally resulted in elimination of all but the usual large divergences at the extremes of the spectrum (Figures 8 and 9).

In the case of small damping, negative-going fluorescence at small times appeared to be unavoidable, as discussed in the text.

References and Notes

(1) Kennard, E. H. *Phys. Rev.* **1918**, *11*, 29. Kennard, E. H. *Phys. Rev.* **1926**, *28*, 672.

(2) Stepanov, B. I. *Dokl. Akad. Nauk SSSR* **1957**, *112*, 839 [*Sov. Phys. Dokl.* **1957**, *2*, 81].

(3) McCumber, D. E. *Phys. Rev.* **1964**, *136*, A954.

(4) Neporent, B. S. *Dokl. Akad. Nauk SSSR* **1958**, *119*, 682 [*Sov. Phys. Dokl.* **1958**, *3*, 337].

(5) Sawicki, D. A.; Knox, R. S. *Phys. Rev. A* **1996**, *54*, 4837.

(6) Becker, M.; Nagarajan, V.; Parson, W. W. *J. Am. Chem. Soc.* **1991**, *113*, 6840.

(7) Croce, R.; Zucchelli, G.; Garlaschi, F. M.; Bassi, R.; Jennings, R. C. *Biochemistry* **1996**, *35*, 8572. Zucchelli, G.; Garlaschi, F. M.; Croce, R.; Bassi, R.; Jennings, R. C. *Biochim. Biophys. Acta* **1995**, 1229, *59*.

(8) Dau, H.; Sauer, K. *Biochim. Biophys. Acta* **1996**, 1273, *175*.

(9) Knox, R. S. *Acta Phys. Pol., A* **1999**, *95*, 85.

(10) Knox, R. S.; Brown, J. S.; Laible, P. D.; Talbot, M. F. J. *Photosyn. Res.* **1999**, *60*, 165.

(11) Huang, K.; Rhys, A. *Proc. R. Soc. (London) A* **1950**, *204*, 406.

(12) Lax, M. *J. Chem. Phys.* **1952**, *20*, 1752.

(13) Mahan, G. D. *Many-Particle Physics*; Plenum Press: New York, 1981.

(14) Mukamel, S. *Principles of Nonlinear Optical Spectroscopy*; Oxford University Press: New York, 1995.

(15) Weiss, U. *Quantum Dissipative Systems*; World Scientific: Singapore, 1993.

(16) Grabert, H.; Schramm, P.; Ingold, G.-L. *Phys. Rep.* **1988**, *168*, 115.

(17) Chernyak, V.; Mukamel, S. *J. Chem. Phys.* **1996**, *105*, 4565.

(18) Jackson, J. D. *Classical Electrodynamics*, 2nd Ed.; John Wiley & Sons: New York, 1975.

(19) Caldeira, A. O.; Leggett, A. J. *Physica A* **1983**, *121*, 587.

(20) Knox W. H.; Teegarden, K. J. *J. Lumin.* **1983**, *31/32*, 39.

(21) Pullerits, T.; Monshouwer, R.; van Mourik, F.; van Grondelle, R. *Chem. Phys.* **1995**, *194*, 395.

(22) Ford, G. W.; Kac, M.; Mazur, P. *J. Math. Phys.* **1965**, *6*, 504.

(23) Ford, G. W.; Kac, M. *J. Stat. Phys.* **1987**, *46*, 803.

(24) Cortés, E.; West, B. J.; Lindenberg, K. *J. Chem. Phys.* **1985**, *82*, 2708.

(25) Dwight, H. B. *Table of Integrals and Other Mathematical Data*; The Macmillian Company: New York, 1961.

(26) Berens, P. H.; Mackey, D. H. J.; White, G. M.; Wilson, K. R. *J. Chem. Phys.* **1983**, *79*, 2375.

(27) Gertner, B. J.; Wilson, K. R.; Hynes, J. T. *J. Chem. Phys.* **1989**, *90*, 3537.

(28) Cao, J.; Messina, M.; Wilson, K. R. *J. Chem. Phys.* **1996**, *106*, 5239.

(29) Zhao, Y.; Chernyak, V.; Mukamel, S. *J. Phys. Chem. A* **1998**, *102*, 6614.

(30) Chang, L.-D.; Chakravarty, S. *Phys. Rev. B* **1985**, *31*, 154.

(31) Knox, R. S.; Marshall, L. F. *J. Lumin.* **2000**, *85*, 209.

(32) Mukamel, S.; Rupasov, V. *Chem. Phys. Lett.* **1995**, *242*, 17.

(33) Mukamel, S. *J. Chem. Phys.* **1997**, *107*, 4165.

(34) Mukamel, S.; Ciordas-Ciurdariu, C.; Khidekel, V. In *Advances in Chemical Physics, Volume 101: Chemical Reactions and Their Control on the Femtosecond Time Scale, XXth Solvay Conference on Chemistry*; Gaspard, P. et al., Eds.; Wiley: New York, 1997; p 345.

(35) Weisstein, E. W. *The CRC Concise Encyclopedia of Mathematics*, CRC Press: Boca Raton, FL, 1998.

(36) Kölbig, K. S. *Computer Phys. Comm.* **1972**, *4*, 221.